Title

Comparison of Fused-Ring Electron Acceptors with One- and Multidimensional Conformations

Journal

ACS Applied Materials & Interfaces, 12(21)

ISSN

1944-8244

Authors

Li, Tengfei

Yang, Langxuan

Wu, Yao

et al.

Publication Date

2020-05-27

DOI

10.1021/acsami.0c04674

Peer reviewed

Comparison of Fused-Ring Electron Acceptors with One- and Multidimensional Conformations

Tengfei Li,[‖] Langxuan Yang,[‖] Yao Wu, Jiayu Wang, Boyu Jia, Qin Hu, Thomas P. Russell, and Xiaowei Zhan*

ABSTRACT: Three fused-ring electron acceptors (FXIC-1, FXIC-2, and FXIC-3) were designed and synthesized. This FXIC series has similar electron-rich central units and the same electron-poor termini. Due to the different steric structures of fluorene, bifluorenylidene, and spirobifluorene, FXIC-1 is a one- dimensional (1D) crystal, while FXIC-2 and FXIC-3 are multidimensional (MD) amorphous materials. The conformations of the FXIC series have a slight impact on their absorption and energy levels. FXIC-1 has higher electron mobility than FXIC-2 and FXIC-3. When blending with different polymer donors (PTB7-Th, J71, and PM7), the FXIC-1-based organic solar cells have efficiencies higher than those of the FXIC-2/FXIC-3-based cells. Meanwhile, the ternary-blend cells based on PTB7-Th:F8IC with FXIC-1, FXIC-2, and FXIC-3 show similar efficiencies, which are all better than those of the binary-blend devices.

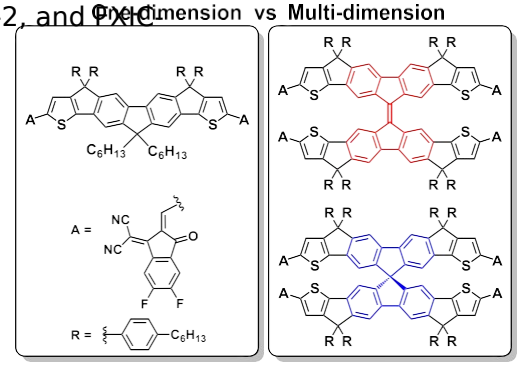

KEYWORDS: *fused-ring electron acceptor, nonfullerene, organic photovoltaics, conformation, multiple dimension*

INTRODUCTION

As a potential approach for capitalizing on solar energy, bulk heterojunction organic solar cells (OSCs) have gained significant interest in the past two decades,[1] since they can be fabricated into lightweight, flexible, semi-transparent, large-area modules by cost-effective printing processes.[2−4] The active layer of OSCs generally contains two types of organic semiconductor materials, electron donor and acceptor. Fullerene derivatives[5] had once been the classical electron acceptor, but their weak absorption, limited electronic tunability, and poor morphological stability limit device performance improvement. To advance this field, it is necessary to develop nonfullerene acceptors that may solve the problems of fullerenes.[6,7]

Since the first report of ITIC[8] in 2015, the development of fused-ring electron acceptors (FREAs) has increased and the efficiency of the OSCs has continually increased.[9−15] In the past five years, a large number of efforts have focused on the design and synthesis of new FREAs by modulating the fused- ring cores,[10,11,16−24] end-capped groups,[25−29] and side chains,[30−33] but most design strategies are based on the same one-dimensional (1D) linear skeletal structures. There has been little effort towards preventing the influence of steric constraints on the performance of nonfullerene acceptors.[23,34] However, the molecular conformation can significantly affect the crystallinity and molecular packing, exciton dissociation and carrier transport in active layers, and finally device performance.[35] For instance, perylene diimide (PDI) deriva-

tives, a class of widely used nonfullerene acceptors, have a rigid planar structure and are prone to aggregation,[7] leading to large crystalline domains and macroscopic phase separation in blend films with insufficient exciton separation. Numerous studies have focused on controlling the crystallinity of the PDI while maintaining efficient charge transport; for example, changing the molecular conformation from 1D to multidimensional (MD) has proven to be a promising strategy.[6,36−39] In FREA materials, 1D linear skeletal structures facilitate the formation of tight molecular packing and large crystalline domains, which is beneficial for charge transport. Meanwhile, the side chains above or below the skeletal plane can adjust the balance between solubility and crystallinity, as well as active-layer morphology. Few reports, though, discuss the fine-tuning of molecular packing and phase separation using different- dimensional FREAs.[23,34]

Herein, we designed and synthesized three new FREAs, FXIC-1−3, with 1D or MD geometries (Chart 1), and explored the effects of steric constraints. These FREAs share similar electron-donating central fused-ring units and the same electron-accepting terminal groups. FXIC-1 contains one

Chart 1. Chemical Structures of the FXIC Series

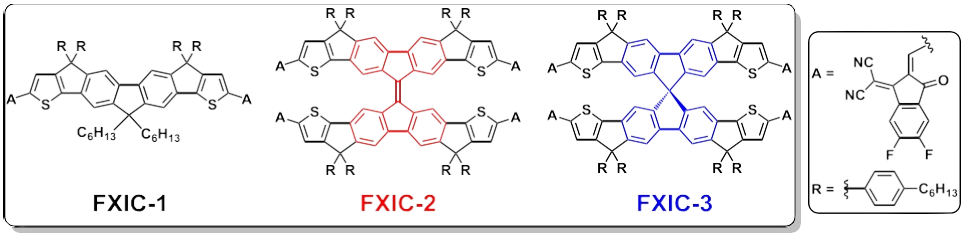

Scheme 1. Synthetic Routes for the FXIC Series

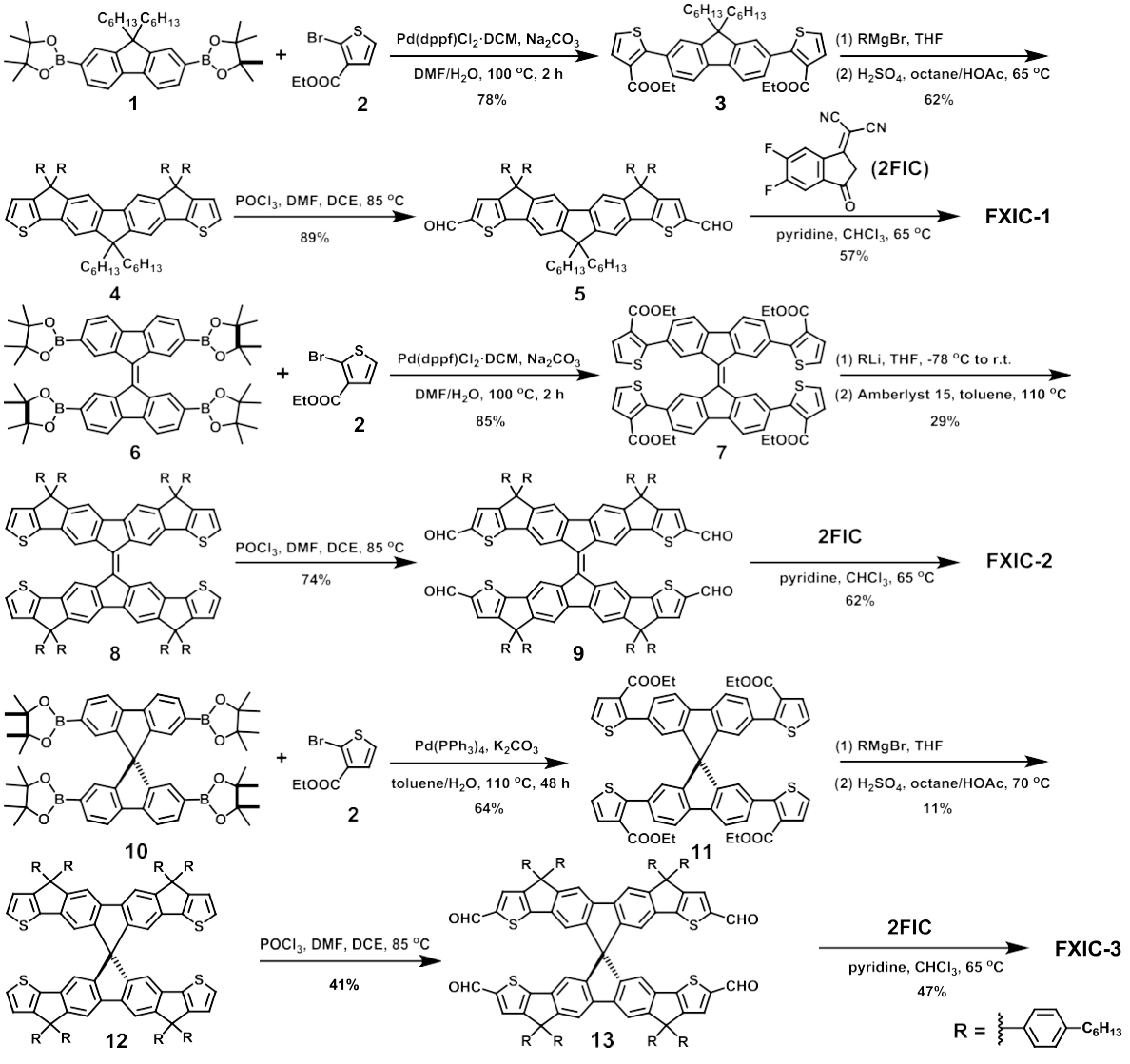

fluorene unit with a regular linear molecular conformation (1D). FXIC-2 has a bifluorenylidene unit with a carbon− carbon double bond connecting two fluorene units, leading to a twisted structure (MD). FXIC-3 contains one spirobifluorene unit where a sp^3-hybrid carbon atom is shared by two fluorene units, leading to an orthogonal structure (MD). The FXIC series shows similar light absorption and frontier molecular orbital energies, but distinct electron mobilities (μ_e). When blending acceptors from the FXIC series with widely used donor materials PTB7-Th,[40] J71,[41] and PM7[42] (Chart S1, Supporting Information), optimized devices based on FXIC-1

show higher power conversion efficiencies (PCEs) than those based on FXIC-2 and FXIC-3. Meanwhile, ternary cells based on PTB7-Th:F8IC:FXIC-1−3 blends have similar PCEs, which are all better than those of the binary blends.

RESULTS AND DISCUSSION

Synthesis and Characterization. Scheme 1 shows the synthetic routes of the FXIC series, and synthesis details are given in the Supporting Information. The FXIC series compounds have good solubility in common organic solvents. We found a partial decomposition of FXIC-2 and FXIC-3

Table 1. Basic Properties of FXIC Series

compound	T_d (°C)	λ_{max}^{abs} (nm) solution	film	E_g[a] (eV)	ε[b] (M^{-1} cm^{-1})	HOMO (eV)	LUMO (eV)	μ[c] (10^{-4} cm^2 V^{-1} s^{-1})
FXIC-1	317	667	684	1.67	2.0×10^5	−5.78	−3.96	5.5 (4.8 ± 0.6)
FXIC-2	245	646	662	1.67	2.4×10^5	−5.79	−4.00	1.8 (1.1 ± 0.7)
FXIC-3	241	651	668	1.68	2.3×10^5	−5.79	−3.98	1.8 (1.2 ± 0.6)

[a]Estimated from the absorption edge in the film. [b]Extinction coefficient at λ_{max} in the solution. [c]Average values with standard deviation in brackets were obtained from six devices.

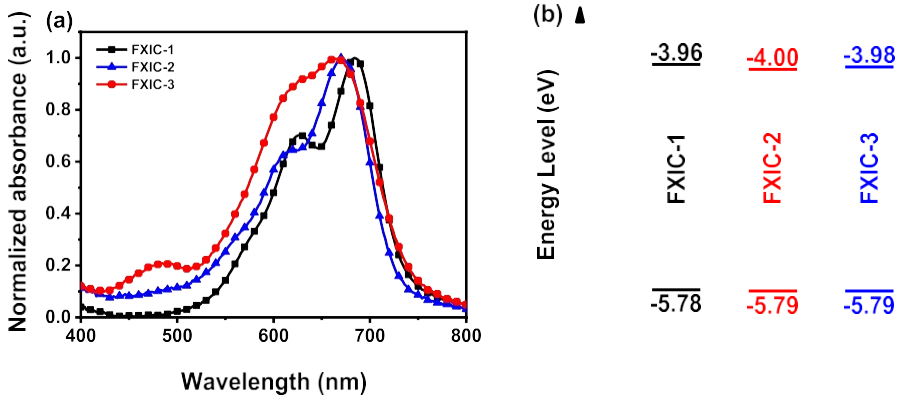

Figure 1. (a) Thin-film absorption spectra and (b) energy levels of FXIC series.

during purification by column chromatography with silica gel, due possibly to a reverse Knoevenagel condensation,[43] while FXIC-1 is relatively stable. The chemical stability of FXIC-1 (1D) with two terminal groups is better than that of FXIC-2/ FXIC-3 (MD) with four terminal groups, which may be caused by the less reverse reaction sites of FXIC-1. The FXIC series compounds have decomposition temperatures (T_d) higher than 240 °C (Figure S1 and Table 1), as determined by thermogravimetric analysis (TGA).

Figure S2 shows the optimized geometries of the FXIC series from theoretical calculations. The electron-rich fused- ring cores of FXIC-1−3 have a 1D planar structure, a twisted structure with a dihedral angle of ca. 35°, and an orthogonal structure. All of the cores and end groups are essentially coplanar, benefiting the electron delocalization and charge transfer. Grazing-incidence wide-angle X-ray scattering (GI-WAXS) was used to determine the molecular stacking of the three materials (Figure S3). FXIC-1 is a crystalline material and shows strong in-plane (100), (200), and (300) reflections at q values of 0.37, 0.74, and 1.12 $Å^{-1}$, respectively, indicating the molecular orientation is “face-on” in the neat film. In contrast, there are no obvious (100) reflections for FXIC-2 and FXIC-3 neat films. FXIC-1−3 show the (010) diffraction peaks at 1.62, 1.46, and 1.45 $Å^{-1}$ (d = 3.87, 4.30, and 4.33 Å, respectively) in the out-of-plane direction, implying that FXIC- 1 has the strongest π−π packing; the trend in π−π packing distances is consistent with the increased twisting of the conformation.

The ultraviolet-visible (UV−vis) absorption spectra of FXIC series in solution and as thin film were measured. In chloroform solution (ca. 10^{-6} M), FXIC-1 shows strong absorption from 550 to 730 nm and a peak at 667 nm with a high molar attenuation coefficient (ε = 2.0×10^5 M^{-1} cm^{-1}), while FXIC-2 and FXIC-3 show blue-shifted peaks at 646 nm with a ε value of 2.4×10^5 M^{-1} cm^{-1} and 651 nm with a ε value of 2.3×10^5 M^{-1} cm^{-1}, respectively (Figure S4a). Thin films of the FXIC series show the main peaks at 684, 662, and

668 nm (Figure 1a), which are all red-shifted by 16−17 nm relative to those in the solution. The band gaps (E_g) of the FXIC series films are 1.67−1.68 eV, calculated from the absorption edges. The conformations of the FXIC series have little influence on their light absorption.

Cyclic voltammetry (CV) (Figure S5) was used to estimate the energy levels of the FXIC series. The highest occupied molecular orbital (HOMO) and the lowest unoccupied molecular orbital (LUMO) energy levels were evaluated using the onset potential of oxidation and reduction, respectively. The compounds in the FXIC series have similar HOMO energy levels (−5.78 to −5.79 eV) and very slightly different LUMO energy levels (−3.96 to −4.00 eV). Consequently, the different conformations of the FXIC series have little impact on their energy levels.

From space-charge-limited current (SCLC) curves (Figure S6),[44] the best μ_e of FXIC-1 (5.5×10^{-4} cm^2 V^{-1} s^{-1}) is greater than those of FXIC-2 and FXIC-3 (1.8×10^{-4} cm^2 V^{-1} s^{-1}). The conformations of the compounds in the FXIC series have a significant influence on the molecular stacking and charge mobilities; FXIC-1 with 1D structure has a tighter stacking, better crystallinity, and higher electron mobility than FXIC-2 and FXIC-3 with a MD structure.

Photovoltaic Performance. To characterize the photovoltaic properties of the FXIC series, the narrow band gap polymer PTB7-Th (1.63 eV), the medium band gap polymer PM7 (1.84 eV), and the wide band gap polymer J71 (1.98 eV) were selected as donors (Figure S4b). The optimization details of PTB7-Th-based devices are summarized in Table S1. The FXIC-1-based cell with 0.2 vol % 1,8-diiodooctane (DIO) had an open-circuit voltage (V_{OC}) of 0.790 V, short-circuit current density (J_{SC}) of 13.4 mA cm^{-2}, fill factor (FF) of 67.4%, and PCE of 7.13%; the FXIC-3-based cell had a lower V_{OC} (0.760 V), lower J_{SC} (12.0 mA cm^{-2}), similar FF (67.4%), and lower PCE (6.12%); and the FXIC-2-based cell had the lowest V_{OC} (0.715 V), the lowest J_{SC} (10.7 mA cm^{-2}), similar FF (68.0%), and the lowest PCE (5.22%) (Figure 2a and Table 2). The

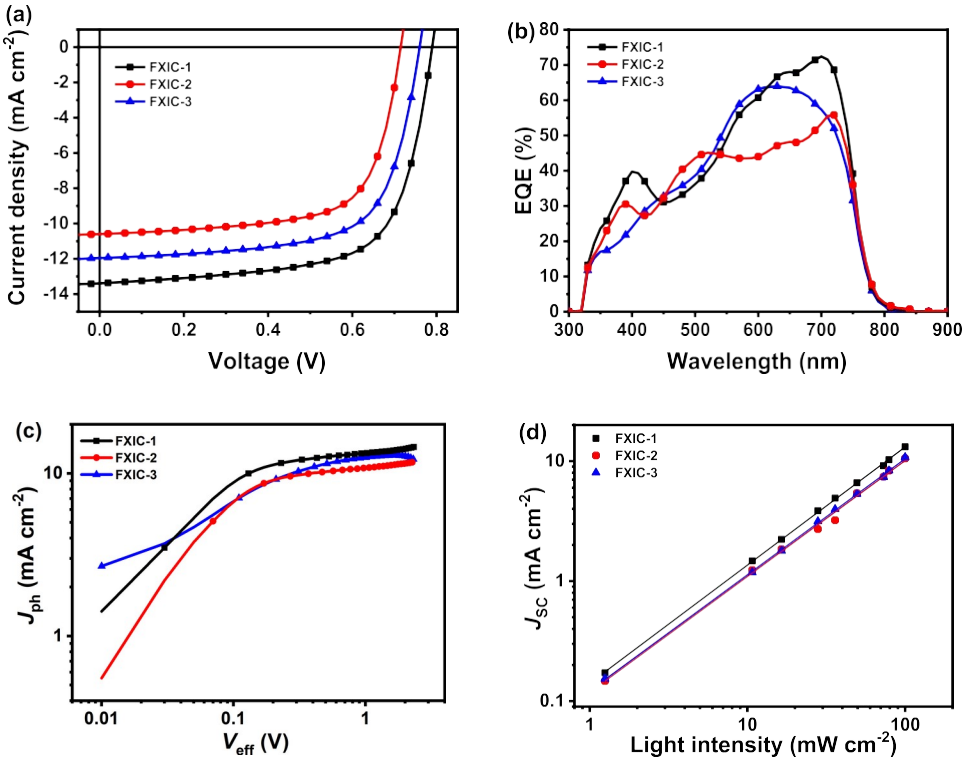

Figure 2. (a) $J-V$ characteristics, (b) EQE spectra, (c) J_{ph} versus V_{eff} characteristics, and (d) J_{SC} versus light intensity of the optimized OSCs based on PTB7-Th:FXIC series.

Table 2. Device Data of Optimized OSCs Based on the PTB7-Th:FXIC Series (1:1.5, w/w)

V_{OC}	acceptor[a]	V [b] (V)	J_{SC} (mA cm^{-2})	FF (%)	PCE (%)	μ_h (10^{-4} cm^2 V^{-1} s^{-1})	μ_e (10^{-4} cm^2 V^{-1} s^{-1})	μ_h/μ_e
0.788	FXIC-1	± 0.005 (0.790)	12.9 ± 0.4 (13.4/13.0[c])	69.4 ± 1.7 (67.4)	7.06 ± 0.09 (7.13)	2.6 ± 0.4 (3.0)	3.5 ± 0.5 (4.0)	0.75
	FXIC-2	± 0.003	10.6 ± 0.2	65.6 ± 1.9	4.96 ± 0.21	0.9 ± 0.3	0.4 ± 0.2	2.

[a]0.2% (v/v) DIO. [b]Average values with standard deviation were obtained from 20 devices, and the values in brackets are from the best device.
[c]From the integration of external quantum efficiency (EQE).

device efficiencies based on 1D FXIC-1 binary blends are higher than those for MD FXIC-2/FXIC-3 binary blends. The binary-blend devices based on J71 and PM7 show a trend similar to that of the PTB7-Th-based cells; the PCEs of 1D FXIC-1-based cells (9.37−10.2%) are higher than those of MD FXIC-2/FXIC-3 (0−6.12%) (Figure S7 and Table S2).

Binary blends of PTB7-Th:FXIC series were investigated to further study the effects of the conformations of the FXIC series on device physics and film morphology. The external quantum efficiency (EQE) of the PTB7-Th:FXIC-1 cell shows the best value with a maximum of 72.5% at 700 nm, while the PTB7-Th:FXIC-2 device shows the lowest EQE in the 500− 700 nm region (Figure 2b), resembling the J_{SC} trend.

Variation in photocurrent density (J_{ph}) with effective voltage (V_{eff}) of the optimized OSCs was investigated, and the ratio of J_{SC}/J_{sat} (J_{sat} is the saturation photocurrent density) was used to probe charge extraction (Figure 2c).[45] The J_{SC}/J_{sat} values of the optimized cells are 0.946, 0.930, and 0.940 for the FXIC-1-, FXIC-2-, and FXIC-3-based devices, respectively. These results indicate efficient charge extraction in all of the devices, essentially independent of the conformations of the FXIC series.

J_{SC} follows a power-law relationship with the incident light

extracted by the electrodes with negligible recombination, α = 1. For binary blends of PTB7-Th:FXIC-1−3, the α values are 0.970, 0.967, and 0.967 under short-circuit conditions (Figure 2d), respectively, suggesting inappreciable bimolecular recom- bination, insensitive to the conformations of the FXIC series. The charge-transport properties of PTB7-Th:FXIC-1−3 blends were studied by SCLC (Figure S8). The PTB7- Th:FXIC-1 blend film shows a hole mobility (μ_h) of 3.0×10^{-4} cm^2 V^{-1} s^{-1} and a μ_e of 4.0×10^{-4} cm^2 V^{-1} s^{-1} with a μ_h/μ_e value of 0.75, while the PTB7-Th:FXIC-3 film exhibits lower charge mobilities with a μ_h/μ_e value of 1.5, and the PTB7- Th:FXIC-2 film exhibits the lowest charge mobilities with a μ_h/μ_e value of 2.1 (Table 2). In contrast to the MD FXIC-2/ FXIC-3-based blends, the 1D FXIC-1-based blends show higher carrier mobilities and more balanced μ_h/μ_e ratios, leading to higher J_{SC}.

intensity (P_{light}): $J_{SC} \propto P^{\alpha}$. If free charges are totally

Film Morphology. The morphology of the blend films was investigated by atomic force microscopy (AFM), GIWAXS, and resonant soft X-ray scattering (R-SoXS). All of the blend films of the PTB7-Th:FXIC series are smooth with root-mean-square roughnesses (R_q) of 2.90, 2.85, and 3.30 nm, respectively (Figure S9). PTB7-Th has an intense in-plane (100) diffraction peak at q = 0.29 $Å^{-1}$ and an out-of-plane (010) stacking reflection at q = 1.66 $Å^{-1}$, indicating a face-on

orientation (Figure S3). In the PTB7-Th:FXIC series binary- blend films, the face-on orientation of PTB7-Th remains when mixed with FXIC-1 and FXIC-3, while the orientation of PTB7-Th changes to edge-on when blended with FXIC-2 due, more than likely, to the strong interactions with FXIC-2 (Figure 3). Out-of-plane (010) reflections are seen at 1.66,

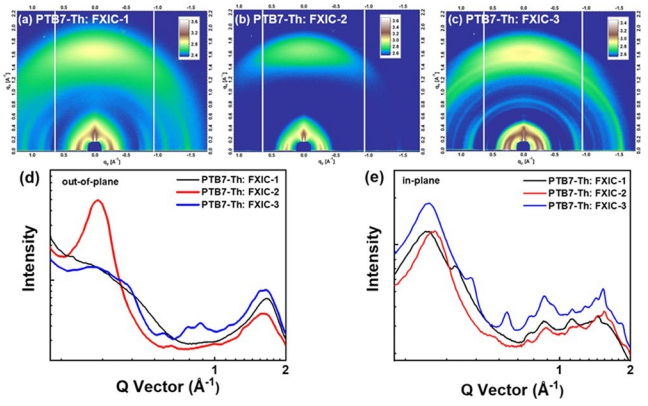

Figure 3. Two-dimensional (2D) GIWAXS patterns (a−c) and scattering profiles of out-of-plane (d) and in-plane (e) peaks for the PTB7-Th:FXIC-1−3 blend films.

1.61, and 1.62 $Å^{-1}$ (d = 3.79, 3.90, and 3.89 Å) for the FXIC-1-, FXIC-2-, and FXIC-3-based blends, respectively. The small π−π packing distance of PTB7-Th:FXIC-1 is favorable for charge transport, contributing to its relatively higher mobilities.

R-SoXS at the carbon edge (285 eV) was performed to investigate the domain sizes of the binary-blend films (Figure 4). The average domain sizes of PTB7-Th:FXIC-1 and PTB7-Th:FXIC-2 are 22 and 20 nm, respectively. PTB7-Th:FXIC-3 shows two interferences at distances corresponding to 43 and 105 nm, indicating that the three-dimensional structure of FXIC-3 hinders mixing with PTB7-Th.[46−48]

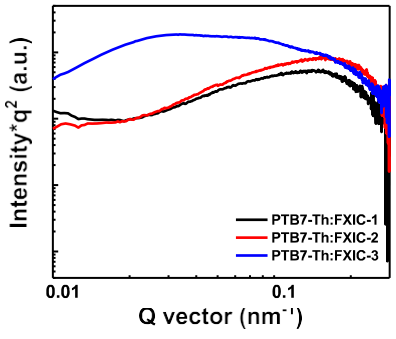

Figure 4. R-SoXS profile in the log scale for the PTB7-Th:FXIC-1−3 blend films.

Ternary-Blend OSCs. We added compounds in the FXIC series to the PTB7-Th:F8IC blends to generate ternary-blend OSCs. The addition of the FXIC series not only supplements the absorption of the binary blend in the 500−750 nm range, enhancing the J_{SC}, but also increases the V_{OC} due to the upshifted LUMO of the FXIC series. We found that the PTB7- Th:F8IC-based devices with 0.2% (v/v) DIO show better performance than those with 0.5% (v/v) diphenyl ether, which we used in our prior work.[49] Therefore, for all of the devices based on PTB7-Th:F8IC:FXIC blends, 0.2 vol % DIO was used as the additive. The devices containing the PTB7-

Th:F8IC binary blend show a PCE of 11.4%, while all of the optimized OSCs for the series of PTB7-Th:F8IC:FXIC ternary blends show higher values for V_{OC}, J_{SC}, and FF, leading to PCEs of 12.4−12.7% (Table S3 and Figure S10). The results indicate that the conformation of the third component has similar effects on the enhancement of device performance. Interestingly, the performance of all of the ternary-blend OSCs is at a high level with high FXIC series loading tolerance.

The influence of the FXIC series on the morphology of the optimized ternary blends was investigated. In contrast to the PTB7-Th:F8IC binary blend that shows a broad peak with a domain size of 24−40 nm, the three ternary blends with different acceptor weight ratios (F8IC:FXIC-1 = 1.3:0.2, F8IC:FXIC-2 = 1.0:0.5, F8IC:FXIC-3 = 1.1:0.4) show broad peaks with a similar domain size of 20−40 nm, indicating that the addition and the weight ratio of the FXIC series have little effect on the domain size (Figure S11). This can explain why the PCEs of the ternary-blend OSCs remain over 10% with high FXIC series loadings. From the GIWAXS of the PTB7-Th:F8IC:FXIC-1 and PTB7-Th:F8IC:FXIC-3 ternary blends, the in-plane (100) peak of F8IC becomes much sharper, indicating that the addition of FXIC-1 and FXIC-3 induces the crystallization of F8IC (Figures S3 and S12). The out-of-plane (010) peaks of FXIC-1, FXIC-2, and FXIC-3 ternary films are located at 1.81, 1.77, and 1.81 $Å^{-1}$ (d = 3.47, 3.55, and 3.47 Å), respectively. The π−π stacking distances of FXIC-1- and FXIC-3-based ternary films are closer than that of the FXIC-2- based one. The smaller π−π packing distance is favorable for charge transport, contributing to the performance of the FXIC-1- and FXIC-3-based ternary devices.

Device Stability. We measured the light stabilities of the ternary-blend OSCs under continuous illumination (AM 1.5G solar simulator, 100 mW cm^{-2}) (Figure S13). After 180 min of continuous illumination, the PCEs of the ternary-blend devices based on FXIC-1, FXIC-2, and FXIC-3 decreased by 15, 17, and 20%, respectively, which are all better than those of the PTB7-Th:F8IC binary-blend OSCs (decreased by 24%). Thermal stability was tested under continuous heating at 100 °C. After 180 min of continuous heating, the PCEs of the ternary-blend devices based on FXIC-1, FXIC-2, and FXIC-3 decreased by 37, 36, and 44%, respectively, which are all better than those of the PTB7-Th:F8IC binary-blend OSCs (decreased by 49%) (Figure S14). The third-component FXIC series improves the device stability; FXIC-1 and FXIC-2 are better than FXIC-3 for stability improvement.

CONCLUSIONS

In summary, we designed and synthesized three FREAs, which have similar fused-ring central units and the same terminal groups. Due to the different steric structures of fluorene, bifluorenylidene, and spirobifluorene, the conformations of these molecules vary from 1D (FXIC-1) to MD (FXIC-2 and FXIC-3). FXIC-1 is crystalline, while FXIC-2 and FXIC-3 are amorphous. The FXIC series FREAs show similar optical absorption and HOMO/LUMO levels. 1D FXIC-1 has tighter stacking, better crystallinity, and higher mobility than MD FXIC-2/FXIC-3. When blending with different polymer donors (PTB7-Th, J71, and PM7), all FXIC-1-based OSCs yield better photovoltaic performance than those based on FXIC-2/FXIC-3. Meanwhile, the ternary cells based on the PTB7-Th:F8IC:FXIC series exhibit similar efficiencies, which are better than that of the PTB7-Th:F8IC control cell. These results indicate that the conformations of the FXIC series have

little impact on the optical and electrochemical properties but significantly influence the molecular packing, film morphology, and electron mobilities, leading to the better performance of 1D FXIC-1 in binary-blend cells and similar positive impact on ternary-blend cells.

EXPERIMENTAL SECTION

The molecular synthesis and characterization and OSC preparation and measurements are provided in the Supporting Information.

AUTHOR INFORMATION

Corresponding Author

Xiaowei Zhan − *Department of Materials Science and Engineering, College of Engineering, Key Laboratory of Polymer Chemistry and Physics of Ministry of Education, Peking University, Beijing 100871, China;* orcid.org/0000-0002- 1006-3342; Email: xwzhan@pku.edu.cn

Authors

Tengfei Li − *Department of Materials Science and Engineering, College of Engineering, Key Laboratory of Polymer Chemistry and Physics of Ministry of Education, Peking University, Beijing 100871, China*

Langxuan Yang − *Department of Materials Science and Engineering, College of Engineering, Key Laboratory of Polymer Chemistry and Physics of Ministry of Education, Peking University, Beijing 100871, China*

Yao Wu − *Department of Polymer Science and Engineering, University of Massachusetts Amherst, Amherst, Massachusetts 01003, United States;* orcid.org/0000-0002-6680-7347

Jiayu Wang − *Department of Materials Science and Engineering, College of Engineering, Key Laboratory of Polymer Chemistry and Physics of Ministry of Education, Peking University, Beijing 100871, China*

Boyu Jia − *Department of Materials Science and Engineering, College of Engineering, Key Laboratory of Polymer Chemistry and Physics of Ministry of Education, Peking University, Beijing 100871, China*

Qin Hu − *Department of Polymer Science and Engineering, University of Massachusetts Amherst, Amherst, Massachusetts 01003, United States; Materials Sciences Division, Lawrence Berkeley National Laboratory, Berkeley, California 94720, United States*

Thomas P. Russell − *Department of Polymer Science and Engineering, University of Massachusetts Amherst, Amherst, Massachusetts 01003, United States; Materials Sciences Division, Lawrence Berkeley National Laboratory, Berkeley, California 94720, United States;* orcid.org/0000-0001- 6384-5826

Author Contributions

‖T.L. and L.Y. contributed equally to this work.

Notes

The authors declare no competing financial interest.

ACKNOWLEDGMENTS

X.Z. thanks the NSFC (Nos. 51761165023 and 21734001).

T.P.R. and Y.W. are supported by the U.S. Office of Naval Research under contract N00014-17-1-2244. Portions of this research were conducted at beamline 7.3.3 and 11.0.1.2 of Advanced Light Source, Materials Science Division, the Molecular Foundry, Lawrence Berkeley National Laboratory, which was supported by the Office of Science, Office of Basic Energy Sciences, of the U.S. Department of Energy under contract DE-AC02-05CH11231. The Supercomputing Center of the Chinese Academy of Sciences is acknowledged for molecular modeling.

REFERENCES

(1) Yu, G.; Gao, J.; Hummelen, J. C.; Wudl, F.; Heeger, A. J. Polymer Photovoltaic Cells: Enhanced Efficiencies via a Network of Internal Donor-Acceptor Heterojunctions. *Science* 1995, *270*, 1789−1791.

(2) Lu, L.; Zheng, T.; Wu, Q.; Schneider, A. M.; Zhao, D.; Yu, L. Recent Advances in Bulk Heterojunction Polymer Solar Cells. *Chem. Rev.* 2015, *115*, 12666−12731.

(3) Yan, C.; Barlow, S.; Wang, Z.; Yan, H.; Jen, A. K.-Y.; Marder, S. R.; Zhan, X. Non-Fullerene Acceptors for Organic Solar Cells. *Nat. Rev. Mater.* 2018, *3*, No. 18003.

(4) Cheng, P.; Li, G.; Zhan, X.; Yang, Y. Next-Generation Organic Photovoltaics Based on Non-Fullerene Acceptors. *Nat. Photonics* 2018, *12*, 131−142.

(5) He, Y.; Li, Y. Fullerene Derivative Acceptors for High Performance Polymer Solar Cells. *Phys. Chem. Chem. Phys.* 2011, *13*, 1970−1983.

(6) Zhang, G.; Zhao, J.; Chow, P. C. Y.; Jiang, K.; Zhang, J.; Zhu, Z.; Zhang, J.; Huang, F.; Yan, H. Nonfullerene Acceptor Molecules for Bulk Heterojunction Organic Solar Cells. *Chem. Rev.* 2018, *118*, 3447−3507.

(7) Wang, J.; Zhan, X. Rylene Diimide Electron Acceptors for Organic Solar Cells. *Trends Chem.* 2019, *1*, 869−881.

(8) Lin, Y.; Wang, J.; Zhang, Z. G.; Bai, H.; Li, Y.; Zhu, D.; Zhan, X. An Electron Acceptor Challenging Fullerenes for Efficient Polymer Solar Cells. *Adv. Mater.* 2015, *27*, 1170−1174.

(9) Meng, L.; Zhang, Y.; Wan, X.; Li, C.; Zhang, X.; Wang, Y.; Ke, X.; Xiao, Z.; Ding, L.; Xia, R.; Yip, H.-L.; Cao, Y.; Chen, Y. Organic and Solution-Processed Tandem Solar Cells with 17.3% Efficiency. *Science* 2018, *361*, 1094−1098.

(10) Wang, J.; Zhang, J.; Xiao, Y.; Xiao, T.; Zhu, R.; Yan, C.; Fu, Y.; Lu, G.; Lu, X.; Marder, S. R.; Zhan, X. Effect of Isomerization on High-Performance Nonfullerene Electron Acceptors. *J. Am. Chem. Soc.* 2018, *140*, 9140−9147.

(11) Yuan, J.; Zhang, Y. Q.; Zhou, L. Y.; Zhang, G. C.; Yip, H. L.; Lau, T. K.; Lu, X. H.; Zhu, C.; Peng, H. J.; Johnson, P. A.; Leclerc, M.; Cao, Y.; Ulanski, J.; Li, Y. F.; Zou, Y. P. Single-Junction Organic Solar Cell with over 15% Efficiency Using Fused-Ring Acceptor with Electron-Deficient Core. *Joule* 2019, *3*, 1140−1151.

(12) Cui, Y.; Yao, H.; Hong, L.; Zhang, T.; Xu, Y.; Xian, K.; Gao, B.; Qin, J.; Zhang, J.; Wei, Z.; Hou, J. Achieving over 15% Efficiency in Organic Photovoltaic Cells via Copolymer Design. *Adv. Mater.* 2019, *31*, No. 1808356.

(13) Xu, X.; Feng, K.; Bi, Z.; Ma, W.; Zhang, G.; Peng, Q. Single- Junction Polymer Solar Cells with 16.35% Efficiency Enabled by a Platinum(II) Complexation Strategy. *Adv. Mater.* 2019, *31*, No. 1901872.

(14) Zhou, Z.; Xu, S.; Song, J.; Jin, Y.; Yue, Q.; Qian, Y.; Liu, F.; Zhang, F.; Zhu, X. High-Efficiency Small-Molecule Ternary Solar

Cells with a Hierarchical Morphology Enabled by Synergizing Fullerene and Non-Fullerene Acceptors. *Nat. Energy* 2018, *3*, 952−959.

(15) Li, X.; Pan, F.; Sun, C.; Zhang, M.; Wang, Z.; Du, J.; Wang, J.; Xiao, M.; Xue, L.; Zhang, Z. G.; Zhang, C.; Liu, F.; Li, Y. Simplified Synthetic Routes for Low Cost and High Photovoltaic Performance N-Type Organic Semiconductor Acceptors. *Nat. Commun.* 2019, *10*, No. 519.

(16) Wang, W.; Yan, C.; Lau, T.-K.; Wang, J.; Liu, K.; Fan, Y.; Lu, X.; Zhan, X. Fused Hexacyclic Nonfullerene Acceptor with Strong Near-Infrared Absorption for Semitransparent Organic Solar Cells with 9.77% Efficiency. *Adv. Mater.* 2017, *29*, No. 1701308.

(17) Li, T.; Dai, S.; Ke, Z.; Yang, L.; Wang, J.; Yan, C.; Ma, W.; Zhan, X. Fused Tris(Thienothiophene)-Based Electron Acceptor with Strong Near-Infrared Absorption for High-Performance As-Cast Solar Cells. *Adv. Mater.* 2018, *30*, No. 1705969.

(18) Zhu, J.; Ke, Z.; Zhang, Q.; Wang, J.; Dai, S.; Wu, Y.; Xu, Y.; Lin, Y.; Ma, W.; You, W.; Zhan, X. Naphthodithiophene-Based Non- fullerene Acceptor for High-Performance Organic Photovoltaics: Effect of Extended Conjugation. *Adv. Mater.* 2018, *30*, No. 1704713.

(19) Xiao, Z.; Jia, X.; Li, D.; Wang, S.; Geng, X.; Liu, F.; Chen, J.; Yang, S.; Russell, T. P.; Ding, L. 26 mA cm^{-2} J_{SC} from Organic Solar Cells with a Low-Bandgap Nonfullerene Acceptor. *Sci. Bull.* 2017, *62*, 1494−1496.

(20) Liu, W.; Zhang, J.; Zhou, Z.; Zhang, D.; Zhang, Y.; Xu, S.; Zhu, X. Design of a New Fused-Ring Electron Acceptor with Excellent Compatibility to Wide-Bandgap Polymer Donors for High-Perform- ance Organic Photovoltaics. *Adv. Mater.* 2018, *30*, No. 1800403.

(21) Sun, J.; Ma, X.; Zhang, Z.; Yu, J.; Zhou, J.; Yin, X.; Yang, L.; Geng, R.; Zhu, R.; Zhang, F.; Tang, W. Dithieno[3,2-*b*:2′,3′-*d*]Pyrrol Fused Nonfullerene Acceptors Enabling over 13% Efficiency for Organic Solar Cells. *Adv. Mater.* 2018, *30*, No. 1707150.

(22) Yao, Z.; Liao, X.; Gao, K.; Lin, F.; Xu, X.; Shi, X.; Zuo, L.; Liu, F.; Chen, Y.; Jen, A. K. Dithienopicenocarbazole-Based Acceptors for Efficient Organic Solar Cells with Optoelectronic Response over 1000 nm and an Extremely Low Energy Loss. *J. Am. Chem. Soc.* 2018, *140*, 2054−2057.

(23) Cai, G.; Wang, W.; Zhou, J.; Xiao, Y.; Liu, K.; Xie, Z.; Lu, X.; Lian, J.; Zeng, P.; Wang, Y.; Zhan, X. Comparison of Linear- and Star- Shaped Fused-Ring Electron Acceptors. *ACS Mater. Lett.* 2019, *1*, 367−374.

(24) Jia, B.; Wang, J.; Wu, Y.; Zhang, M.; Jiang, Y.; Tang, Z.; Russell, T. P.; Zhan, X. Enhancing the Performance of a Fused-Ring Electron Acceptor by Unidirectional Extension. *J. Am. Chem. Soc.* 2019, *141*, 19023−19031.

(25) Wu, Y.; Bai, H.; Wang, Z.; Cheng, P.; Zhu, S.; Wang, Y.; Ma, W.; Zhan, X. A Planar Electron Acceptor for Efficient Polymer Solar Cells. *Energy Environ. Sci.* 2015, *8*, 3215−3221.

(26) Dai, S.; Zhao, F.; Zhang, Q.; Lau, T. K.; Li, T.; Liu, K.; Ling, Q.; Wang, C.; Lu, X.; You, W.; Zhan, X. Fused Nonacyclic Electron Acceptors for Efficient Polymer Solar Cells. *J. Am. Chem. Soc.* 2017, *139*, 1336−1343.

(27) Cui, Y.; Yang, C.; Yao, H.; Zhu, J.; Wang, Y.; Jia, G.; Gao, F.; Hou, J. Efficient Semitransparent Organic Solar Cells with Tunable Color Enabled by an Ultralow-Bandgap Nonfullerene Acceptor. *Adv. Mater.* 2017, *29*, No. 1703080.

(28) Xie, D.; Liu, T.; Gao, W.; Zhong, C.; Huo, L.; Luo, Z.; Wu, K.; Xiong, W.; Liu, F.; Sun, Y.; Yang, C. A Novel Thiophene-Fused Ending Group Enabling an Excellent Small Molecule Acceptor for High-Performance Fullerene-Free Polymer Solar Cells with 11.8% Efficiency. *Sol. RRL* 2017, *1*, No. 1700044.

(29) Li, S.; Ye, L.; Zhao, W.; Zhang, S.; Mukherjee, S.; Ade, H.; Hou, J. Energy-Level Modulation of Small-Molecule Electron Acceptors to Achieve over 12% Efficiency in Polymer Solar Cells. *Adv. Mater.* 2016, *28*, 9423−9429.

(30) Lin, Y.; He, Q.; Zhao, F.; Huo, L.; Mai, J.; Lu, X.; Su, C. J.; Li, T.; Wang, J.; Zhu, J.; Sun, Y.; Wang, C.; Zhan, X. A Facile Planar Fused-Ring Electron Acceptor for As-Cast Polymer Solar Cells with 8.71% Efficiency. *J. Am. Chem. Soc.* 2016, *138*, 2973−2976.

(31) Lin, Y.; Zhao, F.; He, Q.; Huo, L.; Wu, Y.; Parker, T. C.; Ma, W.; Sun, Y.; Wang, C.; Zhu, D.; Heeger, A. J.; Marder, S. R.; Zhan, X.
High-Performance Electron Acceptor with Thienyl Side Chains for Organic Photovoltaics. *J. Am. Chem. Soc.* 2016, *138*, 4955−4961.
(32) Yang, Y.; Zhang, Z.-G.; Bin, H.; Chen, S.; Gao, L.; Xue, L.;
Yang, C.; Li, Y. Side-Chain Isomerization on an n-Type Organic Semiconductor ITIC Acceptor Makes 11.77% High Efficiency Polymer Solar Cells. *J. Am. Chem. Soc.* 2016, *138*, 15011−15018.
(33) Li, Y.; Zheng, N.; Yu, L.; Wen, S.; Gao, C.; Sun, M.; Yang, R. A
Simple Phenyl Group Introduced at the Tail of Alkyl Side Chains of Small Molecular Acceptors: New Strategy to Balance the Crystallinity of Acceptors and Miscibility of Bulk Heterojunction Enabling Highly Efficient Organic Solar Cells. *Adv. Mater.* 2019, *31*, No. 1807832.
(34) Radford, C. L.; Hendsbee, A. D.; Abdelsamie, M.; Randell, N. M.; Li, Y.; Toney, M. F.; Kelly, T. L.
Effect of Molecular Shape on the Properties of Non-Fullerene Acceptors: Contrasting Calamitic Versus
3D Design Principles. *ACS Appl. Energy Mater.* 2018, *1*, 6513−6523.
(35) Huang, Y.; Kramer, E. J.; Heeger, A. J.; Bazan, G. C. Bulk
Heterojunction Solar Cells: Morphology and Performance Relation- ships. *Chem. Rev.* 2014, *114*, 7006−7043.
(36) Lin, Y.; Wang, Y.; Wang, J.; Hou, J.; Li, Y.; Zhu, D.; Zhan, X. A
Star-Shaped Perylene Diimide Electron Acceptor for High-Perform- ance Organic Solar Cells. *Adv. Mater.* 2014, *26*, 5137−5142.
(37) Meng, D.; Liu, G.; Xiao, C.; Shi, Y.; Zhang, L.; Jiang, L.;
Baldridge, K. K.; Li, Y.; Siegel, J. S.; Wang, Z. Corannurylene Pentapetalae. *J. Am. Chem. Soc.* 2019, *141*, 5402−5408.
(38) Zhang, J.; Li, Y.; Huang, J.; Hu, H.; Zhang, G.; Ma, T.; Chow,
P. C. Y.; Ade, H.; Pan, D.; Yan, H. Ring-Fusion of Perylene Diimide Acceptor Enabling Efficient Nonfullerene Organic Solar Cells with a Small Voltage Loss. *J. Am. Chem. Soc.* 2017, *139*, 16092−16095.
(39) Wu, Q.; Zhao, D.; Schneider, A. M.; Chen, W.; Yu, L.
Covalently Bound Clusters of Alpha-Substituted PDI-Rival Electron Acceptors to Fullerene for Organic Solar Cells. *J. Am. Chem. Soc.* 2016, *138*, 7248−7251.
(40) Liao, S.-H.; Jhuo, H.-J.; Cheng, Y.-S.; Chen, S.-A. Fullerene
Derivative-Doped Zinc Oxide Nanofilm as the Cathode of Inverted Polymer Solar Cells with Low-Bandgap Polymer (PTB7-Th) for High Performance. *Adv. Mater.* 2013, *25*, 4766−4771.
(41) Bin, H.; Gao, L.; Zhang, Z. G.; Yang, Y.; Zhang, Y.; Zhang, C.;
Chen, S.; Xue, L.; Yang, C.; Xiao, M.; Li, Y. 11.4% Efficiency Non- Fullerene Polymer Solar Cells with Trialkylsilyl Substituted 2D- Conjugated Polymer as Donor. *Nat. Commun.* 2016, *7*, No. 13651.
(42) Fan, Q.; Zhu, Q.; Xu, Z.; Su, W.; Chen, J.; Wu, J.; Guo, X.; Ma, W.; Zhang, M.; Li, Y. Chlorine Substituted 2D-Conjugated Polymer for High-Performance Polymer Solar Cells with 13.1% Efficiency via
Toluene Processing. *Nano Energy* 2018, *48*, 413−420.
(43) Aldrich, T. J.; Matta, M.; Zhu, W.; Swick, S. M.; Stern, C. L.;
Schatz, G. C.; Facchetti, A.; Melkonyan, F. S.; Marks, T. J. Fluorination Effects on Indacenodithienothiophene Acceptor Packing and Electronic Structure, End-Group Redistribution, and Solar Cell
Photovoltaic Response. *J. Am. Chem. Soc.* 2019, *141*, 3274−3287.
(44) Malliaras, G. G.; Salem, J. R.; Brock, P. J.; Scott, C. Electrical
Characteristics and Efficiency of Single-Layer Organic Light-Emitting Diodes. *Phys. Rev. B* 1998, *58*, R13411−R13414.
(45) Faist, M. A.; Shoaee, S.; Tuladhar, S.; Dibb, G. F. A.; Foster, S.;
Gong, W.; Kirchartz, T.; Bradley, D. D. C.; Durrant, J. R.; Nelson, J. Understanding the Reduced Efficiencies of Organic Solar Cells Employing Fullerene Multiadducts as Acceptors. *Adv. Energy Mater.* 2013, *3*, 744−752.
(46) Liu, F.; Wang, C.; Baral, J. K.; Zhang, L.; Watkins, J. J.; Briseno,
A. L.; Russell, T. P. Relating Chemical Structure to Device Performance via Morphology Control in Diketopyrrolopyrrole-
Based Low Band Gap Polymers. *J. Am. Chem. Soc.* 2013, *135*, 19248−19259.
(47) Naveed, H. B.; Ma, W. Miscibility-Driven Optimization of
Nanostructures in Ternary Organic Solar Cells Using Non-Fullerene Acceptors. *Joule* 2018, *2*, 621−641.

(48) Wu, Y.; Wang, Z.; Meng, X.; Ma, W. Morphology Analysis of Organic Solar Cells with Synchrotron Radiation Based Resonant Soft X-Ray Scattering. *Prog. Chem.* 2017, *29*, 93−101.
(49) Dai, S.; Li, T.; Wang, W.; Xiao, Y.; Lau, T.-K.; Li, Z.; Liu, K.; Lu, X.; Zhan, X. Enhancing the Performance of Polymer Solar Cells via Core Engineering of NIR-Absorbing Electron Acceptors. *Adv. Mater.* 2018, *30*, No. 1706571.